Tellus SERIES A DYNAMIC METEOROLOGY AND OCEANOGRAPHY
PUBLISHED BY THE INTERNATIONAL METEOROLOGICAL INSTITUTE IN STOCKHOLM

An adjoint sensitivity-based data assimilation method and its comparison with existing variational methods

By YONGHAN CHOI[1], GYU-HO LIM[1]*, DONG-KYOU LEE[1,2] and XIANG-YU HUANG[3], [1]*School of Earth and Environmental Sciences, Seoul National University, Seoul, Korea*; [2]*Korea US Weather and Climate Center, Seoul, Korea*; [3]*National Center for Atmospheric Research, Boulder, CO, USA*

(Manuscript received 29 May 2013; in final form 19 November 2013)

ABSTRACT

An adjoint sensitivity-based data assimilation (ASDA) method is proposed and applied to a heavy rainfall case over the Korean Peninsula. The heavy rainfall case, which occurred on 26 July 2006, caused torrential rainfall over the central part of the Korean Peninsula. The mesoscale convective system (MCS) related to the heavy rainfall was classified as training line/adjoining stratiform (TL/AS)-type for the earlier period, and back building (BB)-type for the later period. In the ASDA method, an adjoint model is run backwards with forecast-error gradient as input, and the adjoint sensitivity of the forecast error to the initial condition is scaled by an optimal scaling factor. The optimal scaling factor is determined by minimising the observational cost function of the four-dimensional variational (4D-Var) method, and the scaled sensitivity is added to the original first guess. Finally, the observations at the analysis time are assimilated using a 3D-Var method with the improved first guess. The simulated rainfall distribution is shifted northeastward compared to the observations when no radar data are assimilated or when radar data are assimilated using the 3D-Var method. The rainfall forecasts are improved when radar data are assimilated using the 4D-Var or ASDA method. Simulated atmospheric fields such as horizontal winds, temperature, and water vapour mixing ratio are also improved via the 4D-Var or ASDA method. Due to the improvement in the analysis, subsequent forecasts appropriately simulate the observed features of the TL/AS- and BB-type MCSs and the corresponding heavy rainfall. The computational cost associated with the ASDA method is significantly lower than that of the 4D-Var method.

Keywords: ASDA method, 4D-Var, radar data, heavy rainfall, MCS

To access the supplementary material to this article, please see Supplementary files under Article Tools online.

1. Introduction

Bjerknes (1904) noted that enough information on the current state of the atmosphere is essential for predicting the future state of the atmosphere using a numerical model in his first attempt of numerical weather prediction (NWP). Initial conditions for NWP can be improved through a process called data assimilation. Talagrand (1997) pointed out that the purpose of data assimilation is using all the available information to determine the current state of the atmospheric flow as accurately as possible. The available information includes the observations, background, their error statistics, and physical laws that govern the evolution of flow. Through data assimilation, all the information is combined in a statistically optimal way to produce improved initial conditions.

The four-dimensional variational (4D-Var) method (Lewis and Derber, 1985; Le Dimet and Talagrand, 1986) has been studied extensively over the past three decades and is now one of the most sophisticated data assimilation methods. Several operational centres implemented the 4D-Var method in their data assimilation systems, including the European Centre for Medium-Range Weather Forecasts (ECMWF; Rabier et al., 2000), the Met Office (Rawlins et al., 2007), Météo France (Gauthier and Thépaut, 2001), the Japan Meteorological Agency (JMA; Honda et al., 2005),

*Corresponding author.
email: gyuholim@snu.ac.kr

Citation: Tellus A 2014, **66**, 21584, http://dx.doi.org/10.3402/tellusa.v66.21584

Environment Canada (Gauthier et al., 2007), the High-Resolution Limited-Area Model (HIRLAM; Huang et al., 2002), the Naval Research Laboratory Atmospheric Variational Data Assimilation System (NVDAS-AR; Xu et al., 2005), and the Canadian Regional Data Assimilation System (REG-4D; Tanguay et al., 2012). 4D-Var is superior to its predecessor, 3D-Var, in the following respects. First, the observations can be assimilated at the time of their measurement. Second, flow-dependent background error covariance is used implicitly. Third, 4D-Var analysis is more balanced than 3D-Var analysis because a model is used as a constraint in 4D-Var. Despite the many advantages of 4D-Var, however, it is computationally very intensive due to the iterative nature of its minimisation algorithm.

The sensitivity gradient of 48-hours forecast error with respect to the initial condition was calculated by using an adjoint method in Rabier et al. (1996). The forecast error was defined as the difference between the 48-hours forecast and the verifying analysis, which was considered as the truth, and the dry total energy norm was used. This gradient was multiplied by a scaling factor to make a perturbation, and the perturbation was added to the original initial condition. In their study, the scaling factor was derived by trial and error, and the order of magnitude was around 0.01. The forecast starting from the perturbed initial condition, the so-called 'sensitivity integration', was more accurate than the original forecast not only in the short-range but also in the medium-range. However, sensitivity integration did not yield a better forecast than that obtained using the latest initial condition. In other words, sensitivity integration lost its predictive skill by waiting 48 hours to obtain the verifying analysis. Therefore, sensitivity integration could not be used in operational mode; rather it should be used as a diagnostic tool.

The adjoint sensitivity of short-range forecast error to the initial condition can be used as the perturbation which, when scaled appropriately and added to the original initial condition, improves the subsequent forecast and its consistency. However, the forecast from the perturbed initial condition is not better than the forecast starting from the initial condition at the time of the verifying analysis. In order to overcome these limitations, Huang et al. (1997) proposed the Poorman's variational assimilation (PMV) system. The system was a hybrid one based on both an intermittent data assimilation method, an optimal interpolation (OI) scheme, and a variational data assimilation method, a 4D-Var scheme. The main idea of the PMV is using the adjoint model to produce an improved first guess, which leads to an improved OI analysis. Five-day data assimilation experiments revealed that the analysis increments of the PMV were reduced (i.e. closer to the observations) and the subsequent PMV forecasts were improved compared to the OI. However, the PMV violates the basic assumption, that the first-guess error and the observational error should be uncorrelated, although the orthogonality between the barotropic OI analysis and the baroclinic PMV analysis alleviates the problem related to this violation. In Huang (1999), a generalised version of the PMV (GPV), which had implementation flexibility due to its incremental nature, was proposed. Running the variational component at lower resolutions and with a different model formulation did not alter the conclusions of Huang et al. (1997). In other words, the GPV led to smaller analysis increments, modified baroclinic structures at upper levels, and improved forecasts.

Hello et al. (2000) proposed an analysis correction method in which the original analysis was perturbed by adjoint sensitivity to the initial condition, with the sign and magnitude determined by minimising the distance to the available observations at locations where the sensitivity was of significance. In their approach, the response (or objective) function was the mean sea-level pressure, and hence the verifying analysis acting as truth was not necessary. However, if the forecasts from the original analysis are far from the truth, it is difficult to expect a significant improvement in the analysis.

In this study, we propose a new data assimilation method based on the adjoint sensitivity of the forecast error to the initial condition; we refer to this method as the adjoint sensitivity-based data assimilation (ASDA) method. The objectives of this study are to propose a new data assimilation method, namely ASDA, and to compare ASDA with existing data assimilation methods such as 3D-Var and 4D-Var for a heavy rainfall case over the Korean Peninsula. In ASDA, the first-guess error and the observations error are not correlated, unlike in PMV (or GPV), and the computational cost is significantly reduced compared to 4D-Var.

We derived the new data assimilation method based on the adjoint sensitivity of the forecast error in Section 2. In Section 3, we describe our experimental design and a heavy rainfall case. The results of data assimilation experiments are discussed in Section 4. Section 5 presents a summary and conclusions.

2. ASDA method

2.1. Mathematical formulation

Non-linear evolution of a state vector can be expressed as follows using a non-linear model:

$$x_t = M(x_0), \tag{1}$$

where x_t and x_0 are the state vectors at time t (i.e. final time) and 0 (i.e. initial time), and M is a non-linear model. Linear evolution of a small perturbation of the state vector can

be described by a tangent linear model, the first-order derivative of the non-linear model:

$$\delta x_t = \left.\frac{\partial M}{\partial x}\right|_{x=x_0} \delta x_0 = L\delta x_0, \tag{2}$$

where δx_t and δx_0 are the perturbations at time t and 0, and L is a tangent linear model.

A response function, R, is defined as a function of the state vector at time t, and it is differentiable to the state vector.

$$R = f(x_t). \tag{3}$$

Variation of the response function at time t can be derived from Taylor expansion:

$$\Delta R \approx \delta R = \langle \frac{\partial R}{\partial x_t}, \delta x_t \rangle = \langle \frac{\partial R}{\partial x_t}, L\delta x_0 \rangle, \tag{4}$$

where $<,>$ denotes an inner product, and the definition of the tangent linear model is used for the last equality. By using an adjoint relationship,

$$\Delta R \approx \delta R = \langle L* \frac{\partial R}{\partial x_t}, \delta x_0 \rangle, \tag{5}$$

where L^* is an adjoint model.

Variation of the response function at time 0 is as follows:

$$\Delta R \approx \delta R = \langle \frac{\partial R}{\partial x_0}, \delta x_0 \rangle. \tag{6}$$

Consequently, the equation for adjoint sensitivity to the initial condition is derived by equating the right-hand sides of eqs. (5) and (6):

$$\frac{\partial R}{\partial x_0} = L* \frac{\partial R}{\partial x_t}. \tag{7}$$

The above equation implies that the sensitivity gradient of the response function at the initial time can be obtained by running the adjoint model with the sensitivity gradient of the response function at the final time as input.

In this study, forecast error at time t measured in dry total energy is selected as the response function, and the forecast error is defined as the difference between the forecast from time 0 to t and the verifying 3D-Var analysis at time t.

$$R = \frac{1}{2} \langle P(x_t - x_t^{ref}), AP(x_t - x_t^{ref}) \rangle, \tag{8}$$

where x_t is the forecast obtained by running the non-linear model with x_0 as an initial condition, x^{ref} is the verifying analysis, A is a matrix defining the dry total energy norm, and P is a local projection matrix. The above response function can be rewritten as follows.

$$R = \frac{1}{2} \iiint_{\eta,\Sigma} \left[u'^2 + v'^2 + \left(\frac{g}{NT_r}\right)^2 T'^2 + \left(\frac{1}{pc_s}\right)^2 P'^2 \right] d\Sigma d\eta, \tag{9}$$

where u, v, T, and p are the zonal wind, meridional wind, temperature, and pressure components of the state vector, and prime denotes a perturbation. Gravitational acceleration, Brunt-Väisälä frequency, density of air, and speed of sound are denoted by g, N, ρ, and c_s, respectively, and T_r is a reference temperature. The horizontal integration domain defined by the local projection matrix is denoted by Σ, and η is a vertical coordinate.

The adjoint sensitivity of the forecast error to the initial condition given in eq. (7) with the response function of eq. (8) or (9) can be used as a perturbation to improve the original first guess.

$$\delta x_0^{forfg} = \alpha A^{-1} \frac{\partial R}{\partial x_0}, \tag{10}$$

where α is a scaling factor and A^{-1} is for a unit conversion from the adjoint sensitivity to the state vector.

In order to determine the optimal value of the scaling factor, the observational part of the cost function for 4D-Var is minimised using the observations to the final time. It should be noted that the observations at the initial time are excluded in determining the scaling factor.

$$\begin{aligned} J^o(\alpha) = \frac{1}{2} \sum_{i=1}^{t} & \left[H'_i L(t_0, t_i) \alpha A^{-1} \frac{\partial R}{\partial x_0} - d_i^o \right]^T \\ & \times O_i^{-1} \left[H'_i L(t_0, t_i) \alpha A^{-1} \frac{\partial R}{\partial x_0} - d_i^o \right] \\ d_i^o = y_i^o - H_i(M(x_0)), & \end{aligned} \tag{11}$$

where J^o denotes the observational part of the cost function and H' is a linearised version of the observation operator, H. The observation operator computes model equivalents to the observations through a transform from model space to observation space. d^o is an innovation, y^o is an observation, O is an observation error covariance matrix, and subscript i is for the time dimension.

The above cost function is a quadratic function of the scaling factor:

$$J^{o}(\alpha)=\frac{1}{2}\sum_{i=1}^{t}\left[\alpha^{2}\left\{H'_{i}L(t_0,t_i)A^{-1}\frac{\partial R}{\partial x_0}\right\}^{T}\times R_i^{-1}\left\{H'_{i}L(t_0,t_i)A^{-1}\frac{\partial R}{\partial x_0}\right\}-2\alpha\left\{H'_{i}L(t_0,t_i)A^{-1}\frac{\partial R}{\partial x_0}\right\}^{T}R_i^{-1}d_i^{o}+d_i^{oT}R_i^{-1}d_i^{o}\right]. \quad (12)$$

The optimal value of the scaling factor, α_{opt}, which corresponds to the minimum of the cost function, can be found by equating the first-order derivative of the cost function with respect to alpha to zero:

$$J^{o'}(\alpha)=\sum_{i=1}^{t}\left[\alpha\left\{H'_{i}L(t_0,t_i)A^{-1}\frac{\partial R}{\partial x_0}\right\}^{T}\times R_i^{-1}\left\{H'_{i}L(t_0,t_i)A^{-1}\frac{\partial R}{\partial x_0}\right\}-\left\{H'_{i}L(t_0,t_i)A^{-1}\frac{\partial R}{\partial x_0}\right\}^{T}R_i^{-1}d_i^{o}\right]$$

$$\alpha_{opt}=\frac{\sum_{i=1}^{t}\left\{H'_{i}L(t_0,t_i)A^{-1}\frac{\partial R}{\partial x_0}\right\}^{T}R_i^{-1}d_i^{o}}{\sum_{i=1}^{t}\left\{H'_{i}L(t_0,t_i)A^{-1}\frac{\partial R}{\partial x_0}\right\}^{T}R_i^{-1}\left\{H'_{i}L(t_0,t_i)A^{-1}\frac{\partial R}{\partial x_0}\right\}}. \quad (13)$$

Finally, the adjoint sensitivity of the forecast error scaled by the optimal scaling factor is added to the original first guess to make the improved first guess, and 3D-Var analysis is carried out using the improved first guess and the observations at the initial time to make the improved analysis.

$$x_0^{\text{new fg}}=x_0+\delta x_0^{\text{for fg}}=x_0+\alpha_{opt}A^{-1}\frac{\partial R}{\partial x_0}, \quad (14)$$

$$\delta x_0^{ASDA}=\text{minimizer of } J^{3dvar}(\delta x)$$
$$J^{3dvar}(\delta x)=\frac{1}{2}(\delta x)^{T}B^{-1}\delta x+\frac{1}{2}(H'\delta x-d^{o})^{T}O^{-1}(H'\delta x-d^{o})$$
$$d^{o}=y^{o}-H(x_0^{newfg}), \quad (15)$$

$$x_0^{ASDA}=x_0^{\text{new fg}}+\delta x_0^{ASDA}, \quad (16)$$

where $x^{\text{new fg}}$ is the improved first guess for 3D-Var analysis at the initial time, J^{3dvar} is a cost function for 3D-Var at the initial time, and x^{ASDA} is the final initial condition (analysis) of the ASDA method.

2.2. *Characteristics of the ASDA method*

Figure 1 shows a schematic diagram for the ASDA method. In the ASDA method, an analysis is obtained by the following procedure.

(1) A non-linear model with full physics schemes is run from $t=0$ to $t=30$ minutes (here, an assimilation window of 30 minutes is assumed) with the original first guess (x_0) as an initial condition.
(2) A 3D-Var analysis is performed using the observations at 30 minutes and the forecast from step 1 to produce the reference state (x^{ref}).
(3) A forecast error is defined as the difference between the forecast from step 1 and the reference state from step 2. A response function is calculated using eq. (9), and an adjoint model is run backwards from $t=30$ minutes to $t=0$ to produce an adjoint sensitivity of forecast error at $t=0$ ($\partial R/\partial x_0$).
(4) A scaling factor (α) is determined by minimising eq. (11), and the adjoint sensitivity of the forecast error from step (3) is scaled ($\alpha A^{-1}\partial R/\partial x_0$). It should be noted that the observations at $t=0$ are not used in the determination of the scaling factor. An improved first guess is produced by adding the original first guess and the scaled adjoint sensitivity.
(5) Finally, a 3D-Var analysis is performed using the observations at $t=0$ and the improved first guess from step 4 to produce a final ASDA analysis (x^{ASDA}).

In the PMV method, the observations at the end of the assimilation window are used twice: once for improving the first guess and the other time for making the final PMV analysis. Therefore, in the PMV method, the first-guess and observation errors are correlated with each other. In the ASDA method, the observations at the end of the assimilation window are used for improving the first guess

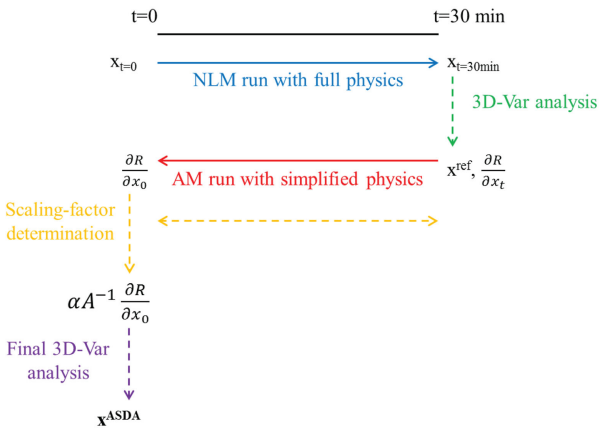

Fig. 1. Schematic diagram for the ASDA method.

like the PMV method, but they are not used for making the final ASDA analysis. It should be also noted that not the background but the first guess is modified using the adjoint sensitivity of forecast error in the ASDA method. These characteristics of the ASDA method ensure the consistency between the background and its error. Additionally, in the ASDA method, the scaling factor is objectively determined by using the observations within the assimilation window (except for the observations at the analysis time).

In the ASDA method, the first guess for the final analysis is improved using the adjoint sensitivity of the forecast error. All the observations within the assimilation window are used at the time of their measurement, and the structure function is flow-dependent like the 4D-Var method. Furthermore, the computational time is significantly reduced in the ASDA method compared to the 4D-Var method because an iterative minimisation is not necessary in the ASDA method.

3. Experimental design and case description

3.1. Experimental design

We used the Weather Research and Forecasting (WRF) model (Skamarock et al., 2008) version 3.4 as a non-linear forecasting model in this study. Figure 2a shows geographical areas of triply nested domains with horizontal resolutions of 54, 18, and 6 km, respectively. The 54-km domain covers East Asia including Korea, Japan, Taiwan, and Eastern China. The 18-km domain covers the Korean Peninsula and surrounding areas, and the 6-km domain focuses on South Korea. The number of horizontal grids for the 54-, 18-, and 6-km domain is 120×102, 121×103, and 121×127, respectively. The number of vertical levels for all the domains is 35, and the model top is set at 50 hPa.

Physical parameterisation schemes used for the non-linear-model run include the WRF Single-Moment 6-class (WSM6) with graupel microphysics scheme (Hong and Lim, 2006), the Kain-Fritsch cumulus parameterisation scheme (Kain, 2004), the Yonsei University (YSU) planetary boundary layer scheme (Hong et al., 2006), the Rapid Radiative Transfer Model (RRTM) longwave radiation scheme (Mlawer et al., 1997), and the Dudhia shortwave radiation scheme (Dudhia, 1989). For tangent linear- and adjoint-model runs, the simplified linearised physics schemes introduced in Zhang et al. (2013) are used. The National Centers for Environmental Prediction (NCEP) Final Analysis (FNL) data are used as initial conditions for all the domains and lateral boundary conditions for the 54-km domain. Lateral boundary conditions for the 18- and 6-km domains are from model outputs of the 54- and 18-km domains respectively (i.e. one-way nesting method is used). The initial time for the forecast of the 54-, 18-, and 6-km domain is 0000 UTC, 1200 UTC, and 1800 UTC 26 July 2006, respectively. Data assimilation is conducted only on the 6-km domain and 18-h forecast from 1800 UTC 26 to 1200 UTC 27 July 2006 will be analysed throughout the paper.

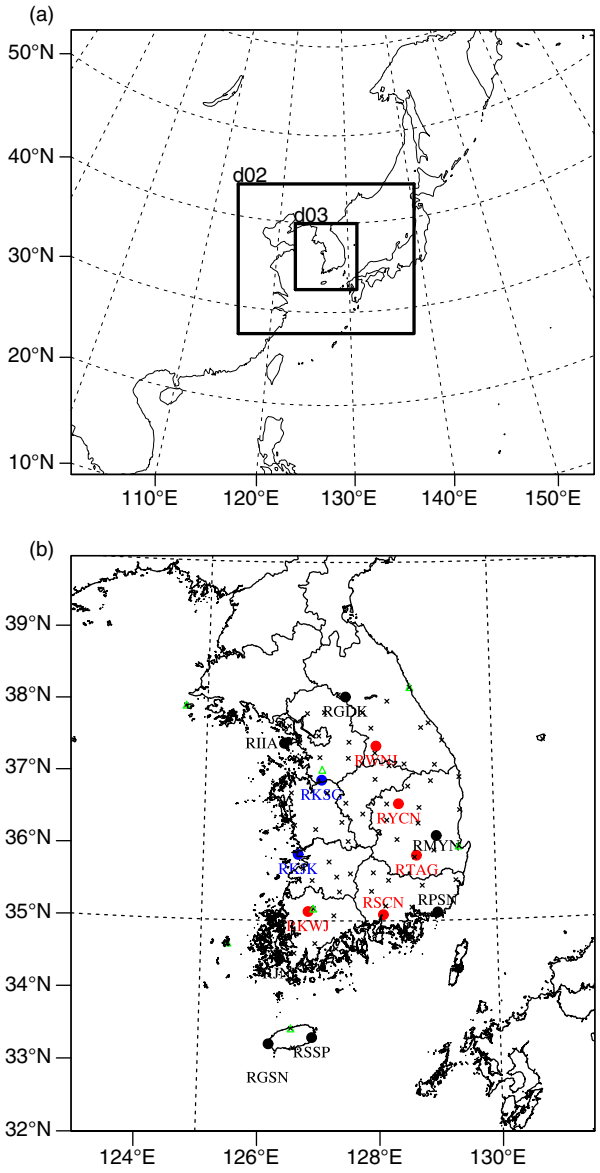

Fig. 2. (a) Geographical areas of domains 1, 2, and 3 and (b) locations of radar observation sites operated by Korea Meteorological Administration (black), Korea Air Force (red), and United States of America Air Force (blue). Locations of automatic weather station (black cross) and radiosonde (green triangle) observation sites over South Korea are also indicated.

In this study, the WRF Data Assimilation (WRFDA) system version 3.4 (Barker et al., 2012), including 3D-Var and 4D-Var capabilities, was used. The initial condition for the experiment without data assimilation (CONTROL experiment in Table 1) is used as a first guess for all the

Table 1. Brief description of numerical experiments

Experiment name	Data assimilation method	Analysis time
CONTROL	–	–
3DVAR	3D-Var	1800 UTC 26 July 2006
4DVAR	4D-Var	1800 UTC 26 July 2006
ASDA	ASDA (proposed in this study)	1800 UTC 26 July 2006
3DVAR_30min	3D-Var	1830 UTC 26 July 2006
PMV	PMV (Huang et al., 1997)	1830 UTC 26 July 2006

data assimilation experiments (i.e. cold start). Background error covariance is calculated by using the National Meteorological Center (NMC) method (Parrish and Derber, 1992), where the background error statistics are derived from the differences between the 24- and 12-hours forecasts for the 1-month period of July 2006. Radar radial velocity data from 14 radar observation sites over the Korean Peninsula (Fig. 2b) are used in this study. In advance of being assimilated, radar data are pre-processed using the methods described by Park and Lee (2009). Pre-processing includes quality control, interpolation/thinning to Cartesian grids by the Sorted Position Radar INTerpolation (SPRINT; Mohr and Vaughan, 1979; Miller et al., 1986) and Custom Editing and Display of Reduced Information in Cartesian coordinate (CEDRIC; Mohr et al., 1986) packages, and hole-filling/smoothing by the CEDRIC package. Finally, radar data are converted into input format appropriate to WRFDA. The final radar data have a horizontal resolution of 6 km, a vertical resolution of 0.5 km at heights mainly above approximately 1.5 km (due to topography), and a temporal resolution of 10 minutes. The assumed observational error for radial velocity is 2 m s^{-1}, and the observation operator for radial velocity developed in Xiao et al. (2005) is used.

3.2. *Heavy rainfall case*

Figure 3 shows the 18-hours accumulated rainfall distribution from 1800 UTC 26 to 1200 UTC 27 July 2006. Rainfall was concentrated over the central part of the Korean Peninsula and it was band-shaped. There were two localised rainfall maxima: one at Seoul and the other at Hongcheon. The 18-hours accumulated rainfall amount at Seoul and Hongcheon was 187.5 and 189.0 mm, respectively. The 1-hour accumulated rainfall amount in the time series of rainfall at Seoul and Hongcheon peaked at 0700 UTC and 0900 UTC 27 July 2006 with a maximum rainfall amount of 32.0 and 37.0 mm, respectively (Fig. 8). The horizontal distribution of the 18-hours accumulated rainfall and time

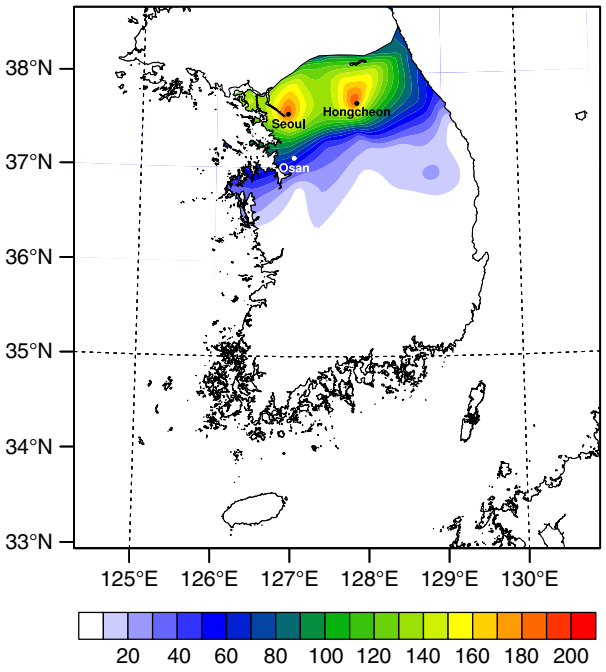

Fig. 3. Observed 18-hours accumulated rainfall (mm $18h^{-1}$) distribution from 1800 UTC 26 to 1200 UTC 27 July 2006. Locations of Seoul, Hongcheon, and Osan are also indicated.

series of rainfall at the two localised maxima will be investigated again in Section 4, being compared with experiment results.

Synoptic environments related to heavy rainfall at 0000 UTC 27 July 2006 are shown in Fig. 4. At 850 hPa, a North Pacific high-pressure system extended to the Korean Peninsula, and this made the atmosphere over the Korean Peninsula very unstable. Warm and moist air was transported to the Korean Peninsula by southerly or southwesterly flow between cyclonic and anti-cyclonic circulations (Fig. 4a). The maximum wind speed of southerly or southwesterly flow was greater than 20 m s^{-1} and hence it could be considered as a low-level jet (LLJ). It is known that low-level convergence appears at the nose of a LLJ, where wind speed decreases abruptly (Astling et al., 1985; McCorcle, 1988; Chen and Kpaeyeh, 1993; Jiang et al., 2007). Over the Yellow Sea, low-level convergence related to a LLJ appeared, and it could provide forcing for upward motion (Fig. 4b). At 500 hPa, a mid-level trough was located west of the Korean Peninsula. Cyclonic vorticity was found over the Yellow Sea although its amplitude was small compared to that related to the low-pressure system (e.g. Aleutian Low; Fig. 4c). The role of this mesoscale convective vortex (MCV) will be investigated in more detail at the end of this sub-section. At 200 hPa, the Korean Peninsula was located on the right of the entrance of an upper-level jet (ULJ), and divergence related to this ULJ was maximised locally over the Yellow

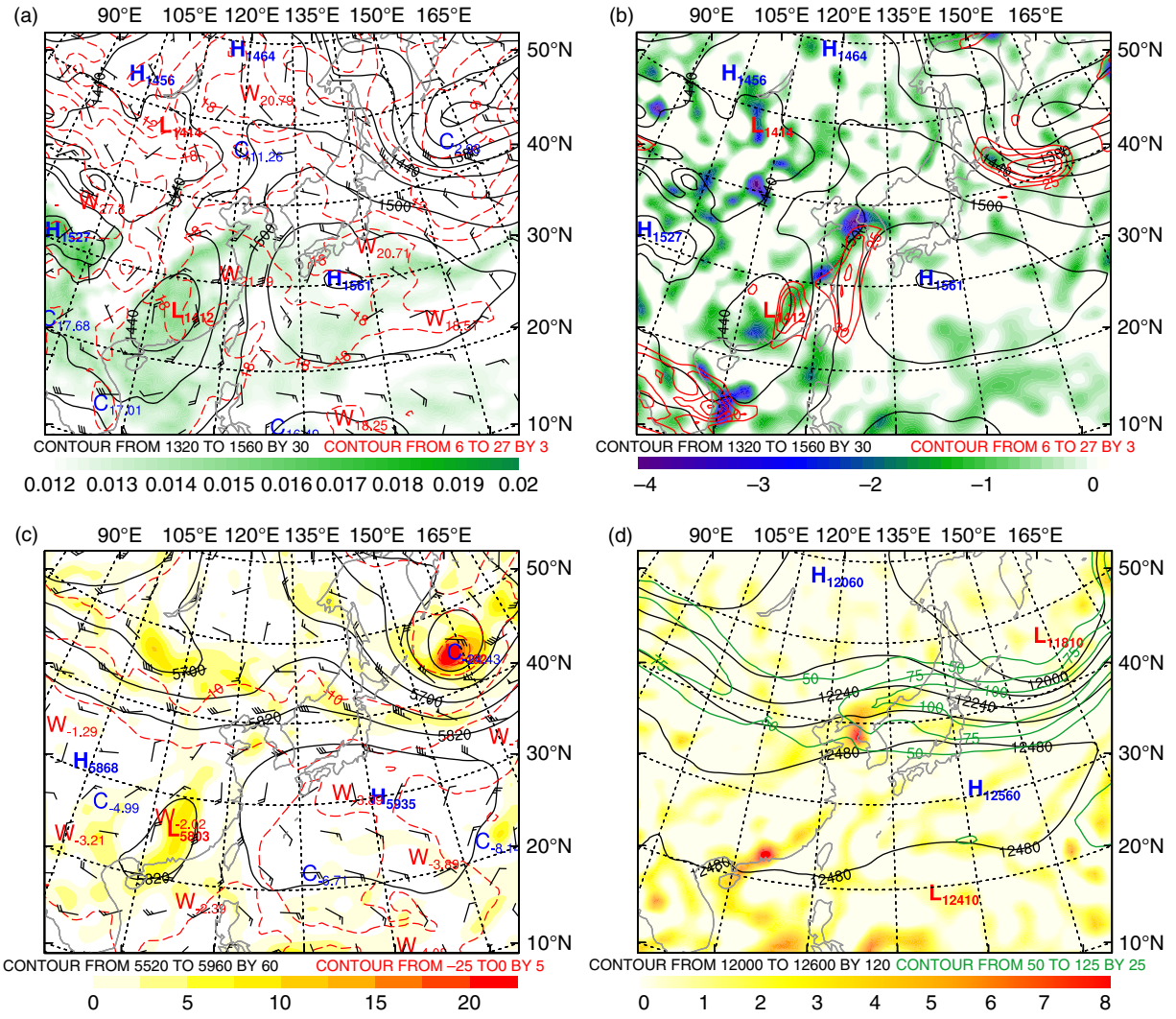

Fig. 4. Synoptic environments at 0000 UTC 27 July 2006. (a) Geopotential height (black solid, contour interval of 30 m), temperature (red dashed, contour interval of 3°C), water vapour mixing ratio (shaded, greater than 0.012 kg kg^{-1}), and wind vector (knot) at 850 hPa, (b) geopotential height (black solid, contour interval of 30 m), wind speed (red solid, contour interval of 5 knots), and divergence (shaded, 10^{-5} s^{-1}, only negative values are plotted) at 850 hPa, (c) geopotential height (black solid, contour interval of 60 m), temperature (red dashed, contour interval of 5°C), relative vorticity (shaded, 10^{-5} s^{-1}, only positive values are plotted), and wind vector (knot) at 500 hPa, (d) geopotential height (black solid, contour interval of 120 m), wind speed (green solid, contour interval of 25 knots), and divergence (shaded, 10^{-5} s^{-1}, only positive values are plotted) at 200 hPa.

Sea (Fig. 4d). Both upper-level divergence related to the ULJ and low-level convergence related to the LLJ were favourable for upward motion, which was essential for the development of mesoscale convective systems (MCSs).

Radar reflectivity and wind vector over the Korean Peninsula at a height of 4-km are provided as a Supplementary file (gif animation). In order to show morphological transitions in MCS development, radar reflectivity and wind vector from 1800 UTC 26 to 1200 UTC 27 July 2006 at an interval of 10-minutes are plotted. From 1800 UTC 26 to 0600 UTC 27 July 2006, the MCS, which affected the Korean Peninsula, could be classified as the training line/adjoining stratiform (TL/AS)-type defined in Schumacher and Johnson (2005). Prolonged heavy convective rainfall was observed along the training (or convective) line and stratiform rainfall was adjacent to the region of convective rainfall. The MCS moved east/northeastward due to west/southwesterly flow over the Korean Peninsula. After 0600 UTC 27, the MCS affecting the Korean Peninsula had characteristics of a back building (BB)-type MCS, also defined in Schumacher and Johnson (2005). Convective cells formed continuously over the west coast of the Korean Peninsula, and they moved eastward slowly. Sometimes they were quasi-stationary and merged

into bigger cells. This characteristic of BB-type MCS, namely linear development and slow movement, caused heavy rainfall over a localised area and in a short period of time.

Figure 5 shows a hodograph and skew T-log p diagram for Osan (refer to Fig. 3 for its location) at 0600 UTC 27 July 2006. The upper-level wind was relatively weak compared to the mid- and lower-level winds. As a result, the wind shear vector reversed its direction sharply with height, and this reversal in the wind shear was reflected by a 'hairpin'-shaped hodograph (Fig. 5a). According to

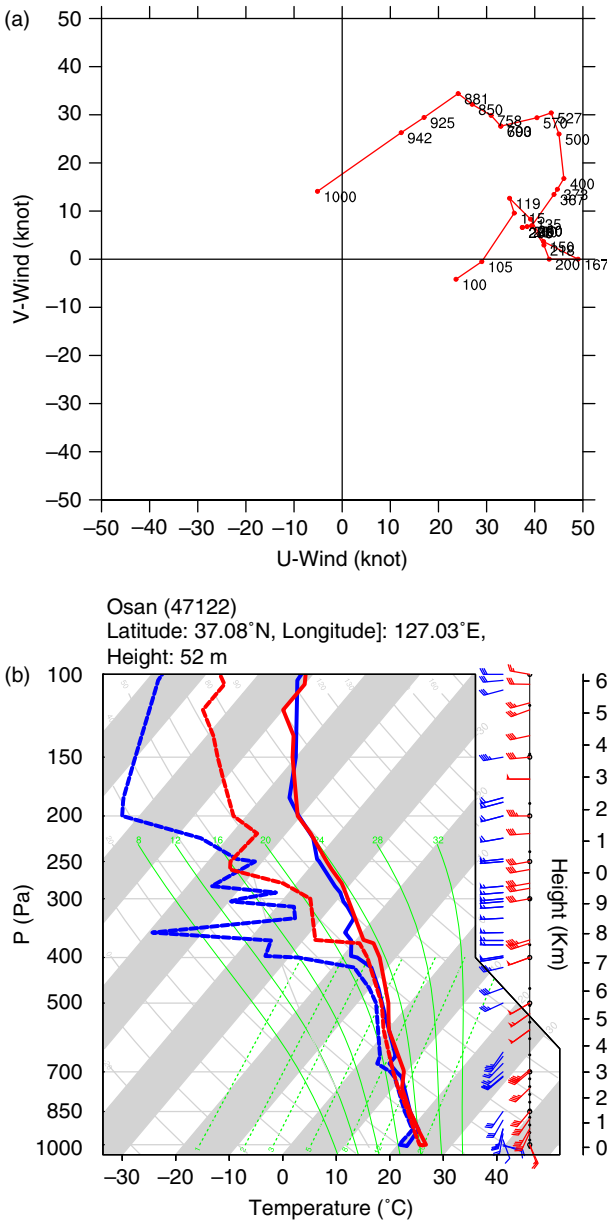

Fig. 5. (a) Hodograph and (b) skew T-log p diagram of Osan at 0600 UTC 27 July 2006.

Schumacher and Johnson (2008, 2009), a MCV interacts with vertical wind shear in the development of a BB-type MCS. In this heavy rainfall case, MCV was generated by prior convective rainfall related to the TL/AS-type MCS, and this MCV interacted with the vertical wind shear. This interaction destabilised the atmosphere by lifting conditionally unstable air (i.e. warm and moist air) to its saturation level, as noted in Schumacher and Johnson (2008, 2009). Due to the vortex-related destabilisation, the convective available potential energy (CAPE) increased from 0 J kg^{-1} to 862 J kg^{-1}, and the convective inhibition (CIN) decreased from -119 J kg^{-1} to -4 J kg^{-1} compared to 0000 UTC 27 (Fig. 5b).

4. Results and discussion

Experiment without data assimilation fails to simulate the heavy rainfall described in Section 3.2. In order to improve the heavy rainfall forecast, radar radial velocity data are assimilated using WRF 3D-Var and 4D-Var systems. Additionally, radar data are assimilated using the proposed ASDA method. Radar data are available every 10 minutes during an assimilation window of 30 minutes from 1800 UTC to 1830 UTC 26 July 2006. Cost function is minimised using a conjugate gradient algorithm with the stopping criterion of a reduction in the gradient norm to 0.01 of its starting value. A brief description of the experiments conducted in this study is given in Table 1.

Before assimilating real observations, pseudo single observation test (PSOT) is carried out to demonstrate how observational data are assimilated in each data assimilation method. A single radial velocity observation at 37.00°N, 127.58°E, 4000 m from the Pyeongtaek radar (located at 36.96°N, 127.02°E, 52 m; RKSG in Fig. 2b) is used for PSOT. The innovation (observation minus background) of the single observation is assigned to 3.10 m s^{-1} for the 3DVAR experiment and 1.51 m s^{-1} for the 4DVAR and ASDA experiments, and the observational error is assumed to 2 m s^{-1}. The single observation is assumed to be at 1930 UTC 26 July 2006, 1.5-h apart from the analysis time, i.e. the assimilation window is from 1800 UTC to 1930 UTC 26 July 2006. Figure 6 shows analysis increments of zonal wind and meridional wind at model level 12 ($\sim$600 hPa) at 1800 UTC 26 July 2006. On the whole, the analysis increments of the ASDA experiment are similar to those of the 4DVAR experiment. In all the experiments, the analysis increments of zonal and meridional winds indicate an anti-cyclonic circulation over the northern side of the radar observation and a cyclonic circulation over the southern side of the radar observation. In the 3DVAR experiment, the analysis increments have their maximum (absolute) values at the observation location.

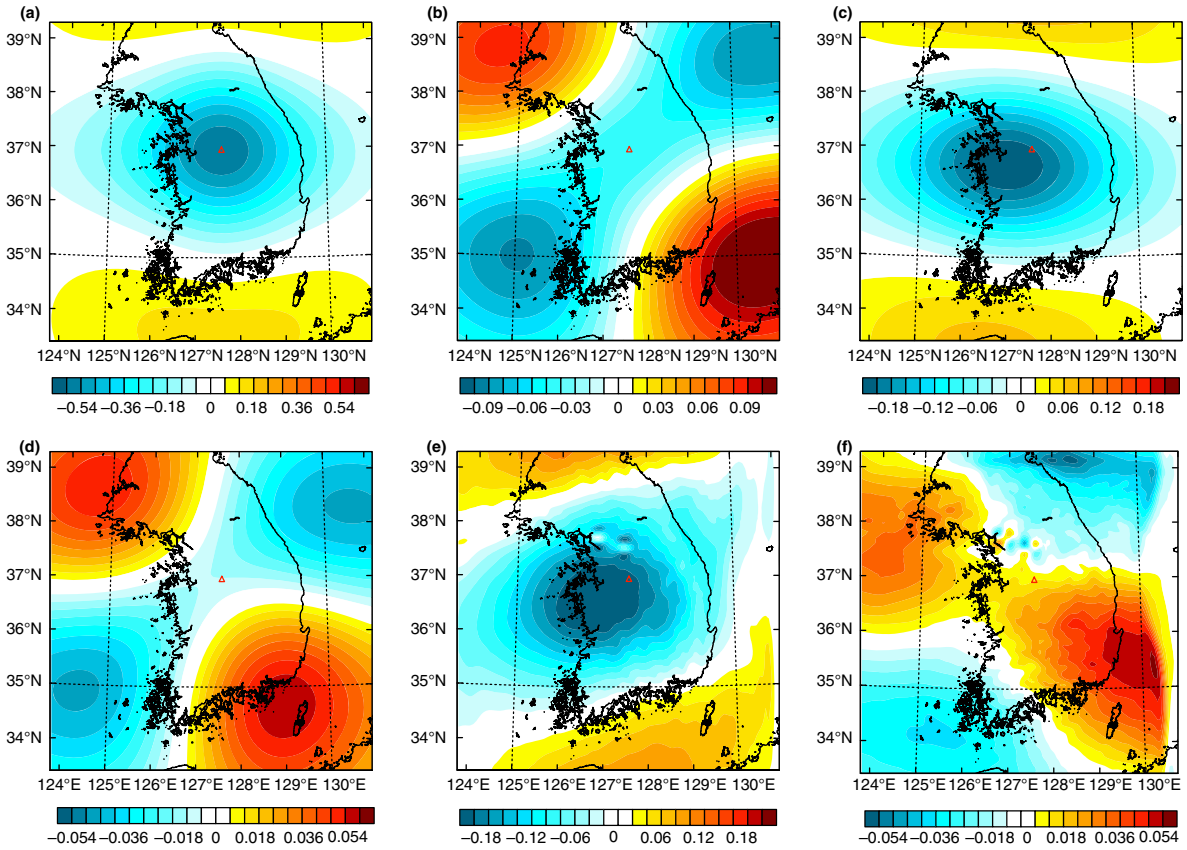

Fig. 6. The analysis increment responses at model level 12 (~600 hPa) to a single radial velocity observation located at 37.00°N, 127.58°E, 4000 m from the Pyeongtaek radar site (36.96°N, 127.02°E, 52 m). The single observation is assumed to be at 1930 UTC 26 July 2006, i.e. the assimilation window is from 1800 UTC to 1930 UTC 26 July 2006. (a) Zonal wind and (b) meridional wind for the 3DVAR experiment, (c) and (d) same as (a) and (b) except for the 4DVAR experiment, (e) and (f) same as (a) and (b) except for the ASDA experiment.

In contrast, in the 4DVAR and ASDA experiments, the maximum (absolute) values of the analysis increments are located in the southwest of the observation location, and their amplitudes are smaller than the 3DVAR experiment. This implies that only in the 4DVAR and ASDA experiments, the innovation is calculated at the time of the measurement. In the 3DVAR experiment, the temperature increment results from the mass-wind balance and Richardson equations. The temperature increment over the northern (southern) side of the radar observation is negative (positive), and its amplitude is small compared to the wind increments. In the 4DVAR and ASDA experiments, the temperature increment in the western half of the domain is negative and the increment in the eastern half of the domain is slightly positive (figures not shown). This structure of the temperature increment is related to the flow pattern over the domain, and hence flow-dependent structure function is used only in the 4DVAR and ASDA experiments. Finally, the analysis increment of water vapour mixing ratio has meaningful amplitude only in the 4DVAR and ASDA experiments (figures not shown). The water vapour increment is created in the 4DVAR and ASDA experiments due to the adjoint-model integration although there is no relationship between wind and water vapour mixing ratio in the background error covariance derived from the NMC method. Consequently, the response to the single radar radial velocity observation in the ASDA experiment is similar to that in the 4DVAR experiment, and different from the 3DVAR experiment.

Figure 7 shows the 18-hours accumulated rainfall distribution from 1800 UTC 26 to 1200 UTC 27 July 2006 for the CONTROL, 3DVAR, 4DVAR, and ASDA experiments. In the CONTROL experiment, the simulated rainfall band is shifted northeastward compared to the observations, and the 18-hours accumulated rainfall amount near Seoul (~93.8 mm) is underestimated (Fig. 7a). When radar radial velocity data are assimilated using the 3D-Var method (3DVAR experiment), the simulated rainfall band is slightly moved southwestward compared to the CONTROL experiment. However, it is still shifted

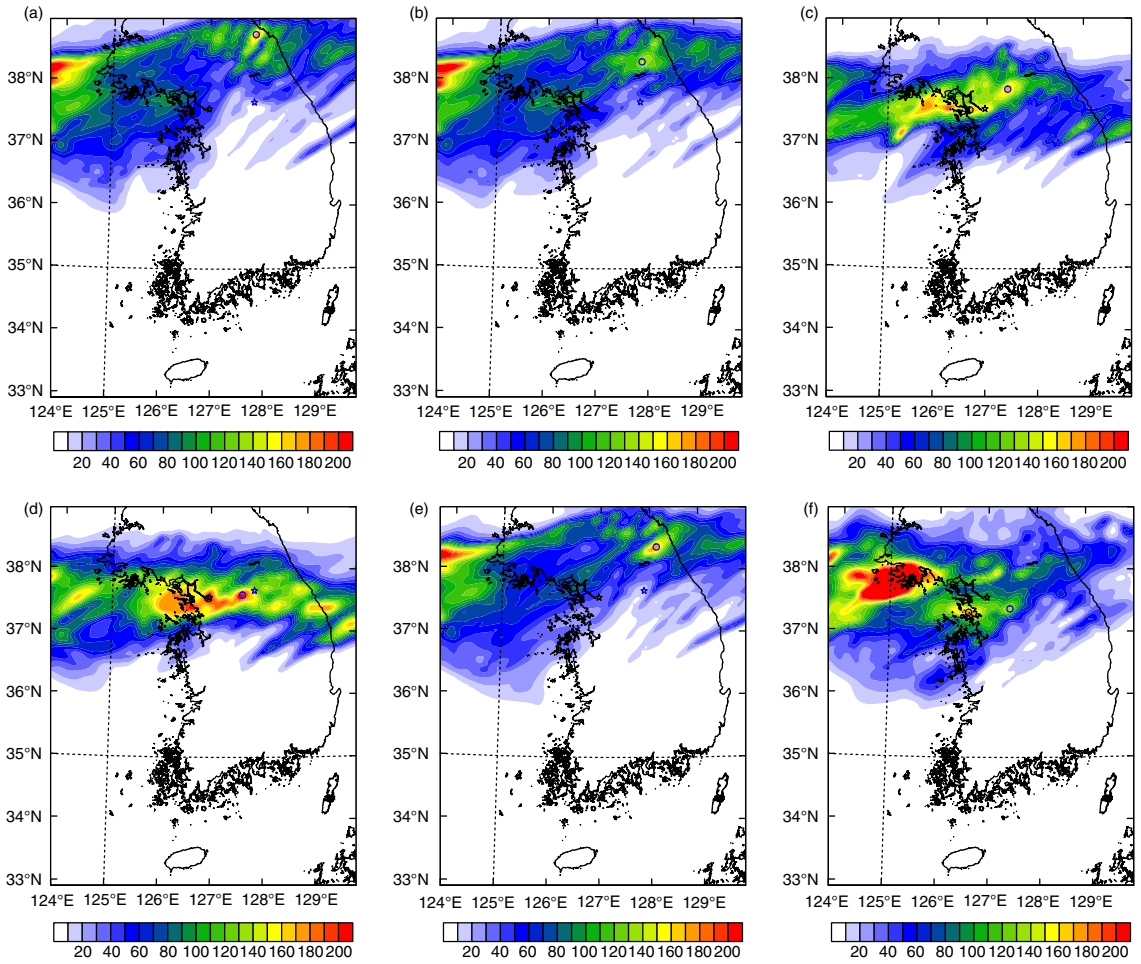

Fig. 7. Eighteen-hours accumulated rainfall (mm $18h^{-1}$) distributions from 1800 UTC 26 to 1200 UTC 27 July 2006 for the (a) CONTROL, (b) 3DVAR, (c) 4DVAR, (d) ASDA, (e) 3DVAR_30min, and (f) PMV experiments.

northeastward compared to the observations, and the 18-hours accumulated rainfall amount near Seoul (~104.2 mm) is also underestimated (Fig. 7b). The simulated rainfall band in the 4DVAR experiment is similar to the observations, and the locations of the two localised rainfall maxima are close to the observations. The 18-hours accumulated rainfall amount at the grid point corresponding to Seoul and Hongcheon is approximately 171.5 and 178.5 mm, respectively. Although the 18-hours accumulated rainfall amount at the points corresponding to Seoul and Hongcheon is underestimated compared to the observations (~187.5 mm and ~189.0 mm), its error is within 10% of the observed value (Fig. 7c). In the ASDA experiment, the rainfall band is well simulated, both in terms of shape and location, when compared to the observations. Especially, the locations of the two localised rainfall maxima are very close to the observations. The 18-hours accumulated rainfall amount at the grid points corresponding to Seoul and Hongcheon is about 205.7 and 216.5 mm, respectively. Compared to the observations, the simulated rainfall amount is slightly overestimated in the ASDA experiment (Fig. 7d). Additionally, two data assimilation experiments are conducted. In the 3DVAR_30min experiment, radar radial velocity data at 1830 UTC 26 July 2006 are assimilated using the 3D-Var method. Radar radial velocity data are assimilated using the PMV method in the PMV experiment. It should be noted that in the 3DVAR_30-min and PMV experiments, the 17.5-hours forecasts are made because the analyses of these experiments are valid at 1830 UTC 26 July 2006. The simulated rainfall distribution in the 3DVAR_30min experiment is similar to the 3DVAR experiment (Fig. 7e). In the PMV experiment, two-branch rainfall band is simulated unlike the observations, and locations of the two localised rainfall maxima are slightly shifted southwestward compared to the observations although the 18-hours accumulated rainfall amount is similar to the observations (Fig. 7f). Hereafter, forecast results of the 3DVAR_30min and PMV experiments will not be mentioned any longer because the main focus of this study is to

compare the ASDA method with the existing variational data assimilation methods, especially the 4D-Var method.

Time series of hourly rainfall amount at the point corresponding to Seoul and Hongcheon for the CONTROL, 3DVAR, 4DVAR, and ASDA experiments is shown in Fig. 8, along with the observations. In the observations at Seoul, the time series of the hourly rainfall was bimodal-shaped, and it peaked at 0700 UTC 27 July 2006 with a rainfall amount of about 32.0 mm. In the CONTROL and 3DVAR experiments, the simulated time series of rainfall is unimodal-shaped, and rainfall peak appears at 0400 UTC and 0500 UTC 27 July 2006 with rainfall amount of about 25.5 and 49.9 mm, respectively. The correlation between the time series of the observations and that of the CONTROL

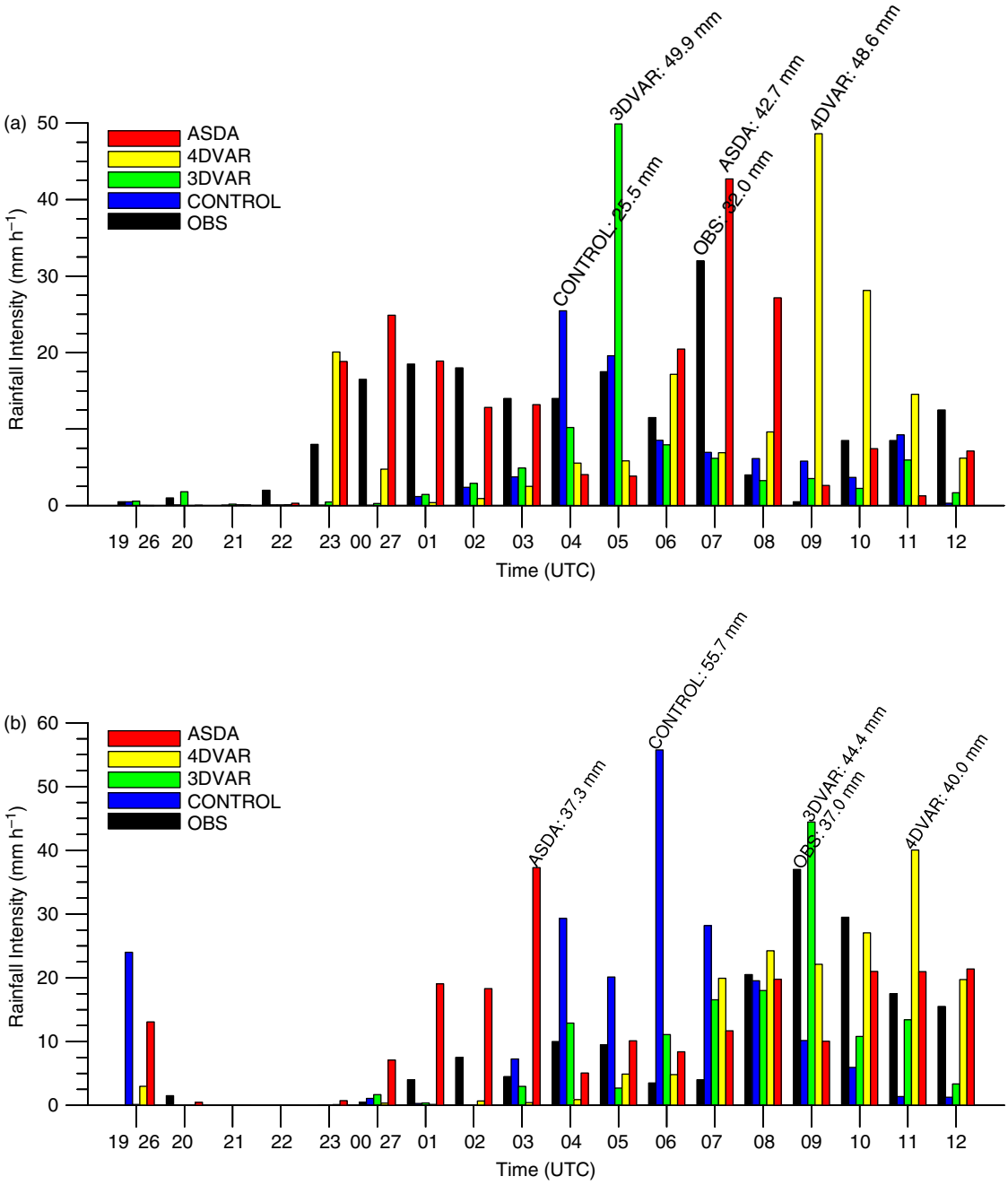

Fig. 8. Time series of hourly rainfall amount (mm h^{-1}) at (a) Seoul and (b) Hongcheon (or the corresponding grid points in case of the model experiment) for the observations (black), CONTROL (blue), 3DVAR (green), 4DVAR (yellow), and ASDA (red) experiments. Maximum hourly rainfall amount is also indicated.

or 3DVAR experiment is 0.295 and 0.298, respectively. In the 4DVAR experiment, the overall pattern of the simulated time series is similar to the observations, and a rainfall peak appears at 0900 UTC 27 July 2006 with a rainfall amount of approximately 48.6 mm. Due to the delay in peak timing, the lag-0 correlation between the observations and the 4DVAR experiment is small, but the lag-2 correlation is about 0.418. The simulated time series of rainfall in the ASDA experiment is similar to the observations with a correlation value of 0.683. The hourly rainfall peaks at 0700 UTC 27 July 2006 like the observations although the peak amount ($\sim$ 42.7 mm) is slightly overestimated compared to the observations. At Hongcheon, the observed time series of rainfall peaked at 0900 UTC 27 July 2006 with a rainfall amount of approximately 37.0 mm. In the CONTROL and 3DVAR experiments, the localised rainfall maximum corresponding to Hongcheon is far from the observations, as can be seen in Fig. 7. The time series of hourly rainfall in the 4DVAR experiment is similar to the observations except for a 2-hour delay in peak timing. The hourly rainfall amount at the peak is about 40.0 mm, which is similar to the observations, and the correlation between the observed time series and the 4DVAR experiment is 0.748. In the ASDA experiment, the overall pattern of time series is well simulated although the correlation coefficient is relatively small ($\sim$0.352) due to overestimation of rainfall at earlier times.

Not only the rainfall forecast but also forecasts of meteorological fields such as winds, temperature, and moisture are improved through radar data assimilation, especially in the 4DVAR and ASDA experiments. Fits to the observations (i.e. biases) of zonal wind, meridional wind, temperature, and water vapour mixing ratio for the CONTROL, 3DVAR, 4DVAR, and ASDA experiments are shown in Fig. 9. Fit to the observations is calculated by using sounding observations from seven radiosonde observations sites (refer to Fig. 2b for their locations) over the Korean Peninsula at 0000 UTC 27 July 2006. Positive biases of zonal wind for the 4DVAR and ASDA experiments are greater than those for the CONTROL and 3DVAR experiments below 800 hPa. However, biases of zonal wind for the 4DVAR and ASDA experiments are smaller than those for the CONTROL and 3DVAR experiments between 800 and 400 hPa, where radar data are relatively plentiful (Fig. 9a). Negative biases of meridional wind below 800 hPa are noticeable in the CONTROL and 3DVAR experiments. These biases are significantly reduced in the 4DVAR and ASDA experiments. Positive biases of meridional wind between 700 and 400 hPa in the 4DVAR and ASDA experiments are slightly reduced compared to those in the CONTROL and 3DVAR experiments (Fig. 9b). Positive (negative) biases of temperature between 800 (600) hPa and 600 (400) hPa are lower in the 4DVAR and ASDA experiments than those in the CONTROL and 3DVAR experiments (Fig. 9c). In all of the experiments, the positive bias of the water vapour mixing ratio prevails throughout the atmosphere (except for 450 hPa in the 4DVAR experiment). These positive biases are remarkably reduced in the 4DVAR and ASDA experiments compared to the CONTROL and 3DVAR experiments, especially below 700 hPa (Fig. 9d). This is related to the large analysis increments of the water vapour mixing ratio over the Yellow Sea (Fig. 11b and 11c) in the 4DVAR and ASDA experiments. On the whole, in terms of fit to the observations, the 4DVAR and ASDA forecasts are improved compared to those of the CONTROL and 3DVAR experiments, particularly at mid-levels where the effects of data assimilation are the greatest. It should also be noted that biases of the meridional wind and water vapour mixing ratio are reduced in the 4DVAR and ASDA experiments, even at lower levels, due to the information-spreading effects of background error covariance and model dynamics.

Figure 10 shows root mean square errors (RMSEs) of radial velocity for the CONTROL, 3DVAR, 4DVAR, and ASDA experiments as a function of forecast length. The RMSE of the radial velocity is calculated by using radar radial velocity observations from 14 radar observation sites over the Korean Peninsula (refer to Fig. 2b) and forecasted radial velocity derived from forecasted wind components. At analysis time (i.e. 1800 UTC 26 July 2006), the RMSE of the radial velocity for the CONTROL, 3DVAR, 4DVAR, and ASDA experiments is 3.10, 2.12, 2.09, and 2.08, respectively. The RMSEs of the data assimilation experiments (RMSE of O–A) are reduced compared to that of the CONTROL experiment (RMSE of O–B). This implies that radar data are assimilated successfully in terms of O–B/O–A statistics in the data assimilation experiments, and the analysis of the ASDA experiment is the closest to the observations at the analysis time. The RMSEs of the radial velocity increase rapidly during the first 6 hours and they oscillate with small amplitude of oscillation in all experiments. Overall, the RMSEs of the radial velocity for the data assimilation experiments are smaller than that for the CONTROL experiment. The RMSEs of the radial velocity for the 4DVAR and ASDA experiments are smaller than that for the 3DVAR experiment, except for the first 2 hours into the forecast. Forecasts of radial velocity in the 4DVAR and ASDA experiments are improved compared to that in the 3DVAR experiment because radar data are assimilated more efficiently in the former two experiments.

In order to investigate the reason why the forecasts of the 4DVAR and ASDA experiments are improved compared to those of the CONTROL and 3DVAR experiments, analysis increments (analysis minus background) of the 4DVAR and ASDA experiments are analysed. Figure 11 shows the horizontal distribution of 850-hPa equivalent

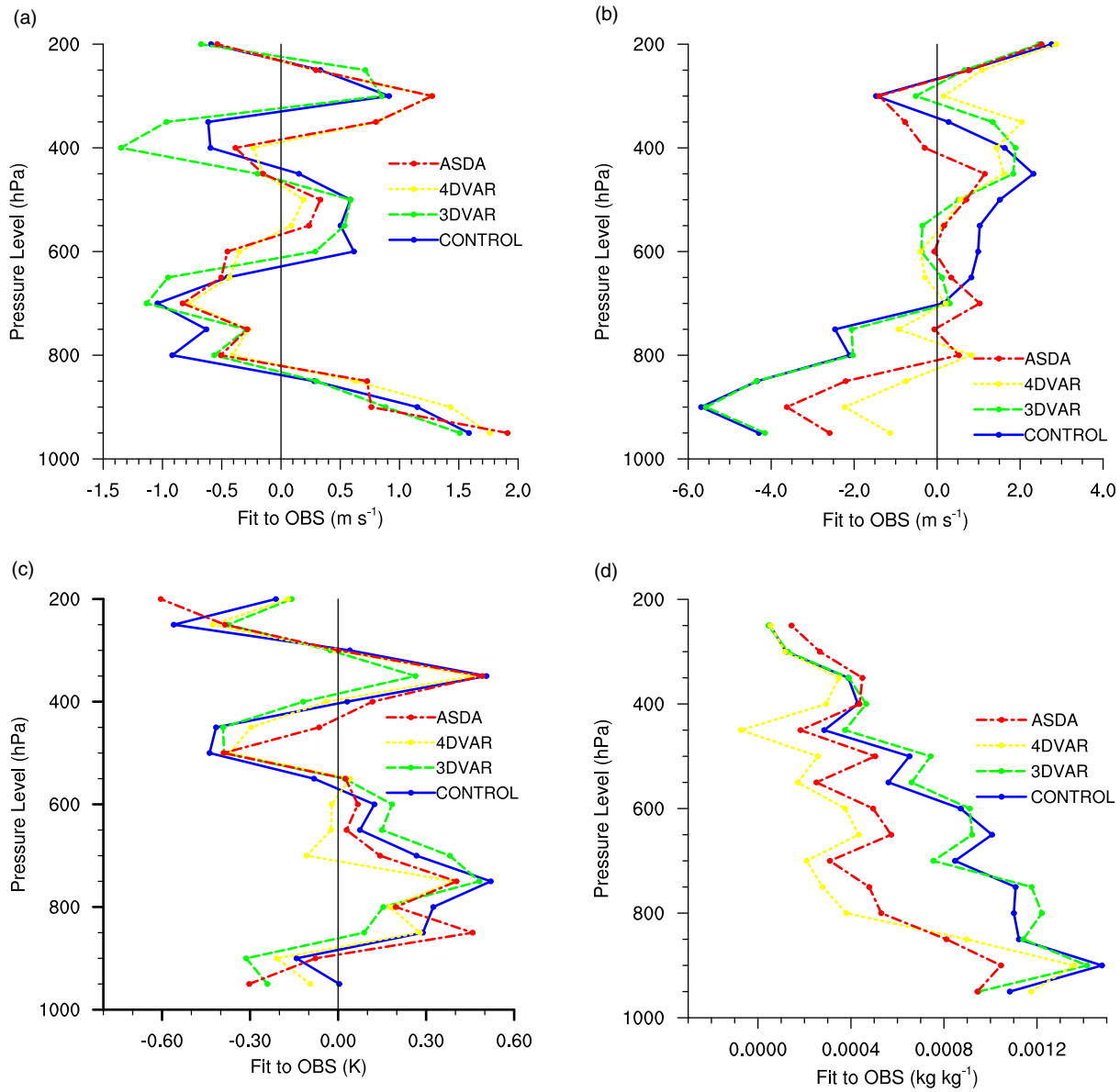

Fig. 9. Vertical distributions of fit to the observations using sounding observations over South Korea at 0000 UTC 27 July 2006 for the CONTROL (blue), 3DVAR (green), 4DVAR (yellow), and ASDA (red) experiments. (a) Zonal wind (m s^{-1}), (b) meridional wind (m s^{-1}), (c) temperature (K), and (d) water vapour mixing ratio (kg kg^{-1}).

potential temperature (EPT) at 1800 UTC 26 July 2006 for the CONTROL, 4DVAR, and ASDA experiments. The analysis increments of EPT for the 4DVAR and ASDA experiments are also shown. In the CONTROL experiment, the meridional gradient of EPT is not large, especially over the central part of the Korean Peninsula (Fig. 11a). However, in the 4DVAR experiment, the meridional gradient of EPT is approximately 44 K over the Yellow Sea. As a result of data assimilation, a negative increment of EPT appears over areas north of 37°N, and a positive increment of EPT appears south of 37°N (Fig. 11b). This change in the EPT field is related to an increase of baroclinic instability over areas upstream of the Korean Peninsula, and it also corrects the location of the surface boundary for TL/AS-type MCS development. It is also noted that the increment of the water vapour mixing ratio is greater than that of temperature. In the ASDA experiment, the meridional gradient of EPT over the Yellow Sea is increased to approximately 16 K although the gradient is not as large as that in the 4DVAR experiment. Unlike the 4DVAR experiment, a positive increment of EPT appears over the continental

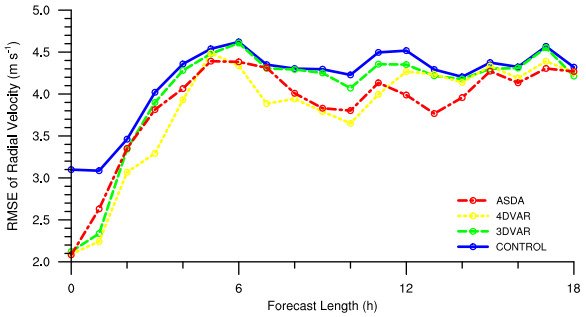

Fig. 10. RMSEs of radial velocity (m s^{-1}) as a function of forecast length for the CONTROL (blue), 3DVAR (green), 4DVAR (yellow), and ASDA (red) experiments. Radar radial velocity data from 14 radar observation sites over the Korean Peninsula are used.

areas north of 37°N (Fig. 11c). This may be partly related to overestimation of rainfall in the ASDA experiment during the early forecast period. Consequently, via data assimilation, the EPT gradient is modified in the 4DVAR and ASDA experiments, and this modification improves rainfall forecast related to the TL/AS-type MCS.

Figure 12 shows horizontal distributions of 500-hPa absolute vorticity and vertical wind shear vectors between 500 and 800 hPa at 0600 UTC 27 July 2006 for the CONTROL, 4DVAR, and ASDA experiments. As explained in Section 3.2, the interaction between MCV and vertical wind shear destabilises the atmosphere by lifting conditionally unstable air to its saturation level. In the CONTROL experiment, until 0600 UTC 27 July 2006, rainfall is concentrated mainly over areas north of 38°N, where transport of warm and moist air by the LLJ is not significant, and hence MCV related to rainfall is also distributed over those areas. This northward-shifted rainfall band in the CONTROL experiment contributes to the failure of simulating BB-type MCS and finally, it results in a northeastward-shifted 18-hours accumulated rainfall distribution. However, in the 4DVAR and ASDA experiments, the movement of the rainfall band from 1800 UTC 26 to 0600 UTC 27 July 2006 is appropriately simulated as in the observations. MCV related to prior rainfall interacts with vertical wind shear over the central part of the Korean Peninsula. As a result of this interaction, warm and moist air transported by the LLJ is lifted, and the atmosphere is destabilised. Consequently, in the 4DVAR and ASDA experiments, conditions for the development of a BB-type MCS are met, and simulated rainfall is concentrated over localised areas after 0600 UTC 27 July 2006 due to the stationarity of a BB-type MCS.

Consequently, in terms of both rainfall forecast and meteorological-field forecast, the 4DVAR and ASDA experiments are superior to the CONTROL or 3DVAR experiment. However, it should be noted that the computational cost of the 4DVAR experiment is much greater than that of the 3DVAR experiment. As a reference to computational cost, detailed running time on a Linux cluster with 8 CPUs and 8-GB memory is given here. A single iteration for the minimisation of the cost function in the 4DVAR experiment takes about 0.5-hours wall clock time (i.e. ~24-hours for a 48-iteration 4D-Var analysis). In contrast, several tens of iterations in the 3DVAR experiment takes less than 5 minutes on the same machine. One-iteration for the minimisation of the cost function in the 4DVAR experiment involves runs of non-linear, tangent linear, and adjoint models, and hence the computational cost of the 4DVAR experiment is much greater than the 3DVAR experiment. The total computational cost of the ASDA experiment is less than 1 hour because the ASDA method does not require iterative minimisation of the cost function.

5. Summary and conclusions

In this study, we selected a heavy rainfall case over the Korean Peninsula that occurred on 1800 UTC 26 July 2006. This case caused torrential rainfall over the central part of the Korean Peninsula. The 18-hours accumulated rainfall amount at Seoul and Hongcheon was 187.5 and 189.0 mm, respectively. Synoptic environments related to the case were favourable for the development of MCSs. At lower levels, warm and moist air was transported to the Korean Peninsula by southerly or southwesterly flow (i.e. LLJ), and this made the atmosphere over the Korean Peninsula conditionally unstable. In addition, low-level convergence related to the LLJ provided consistent forcing for lift. Upper-level divergence related to the ULJ coincided with low-level convergence, and this was responsible for upward motion over the Korean Peninsula.

The MCS related to the heavy rainfall can be classified as TL/AS-type for the period of 1800 UTC 26 to 0600 UTC 27 and BB-type for the period after 0600 UTC 27 July 2006 based on morphological analyses of radar reflectivity. Prolonged heavy convective rainfall was observed along the surface boundary, which was defined by a large EPT gradient, and stratiform rainfall was adjacent to the region of convective rainfall during the TL/AS-type MCS period. MCV induced by prior rainfall interacted with vertical wind shear, and this interaction destabilised the atmosphere over the Korean Peninsula by lifting conditionally unstable air to its saturation level during the BB-type MCS period.

The ASDA method is proposed to evade the high computational cost of the 4D-Var method while retaining the advantages of the 4D-Var method such as flow-dependency and balanced-analysis. In the ASDA method,

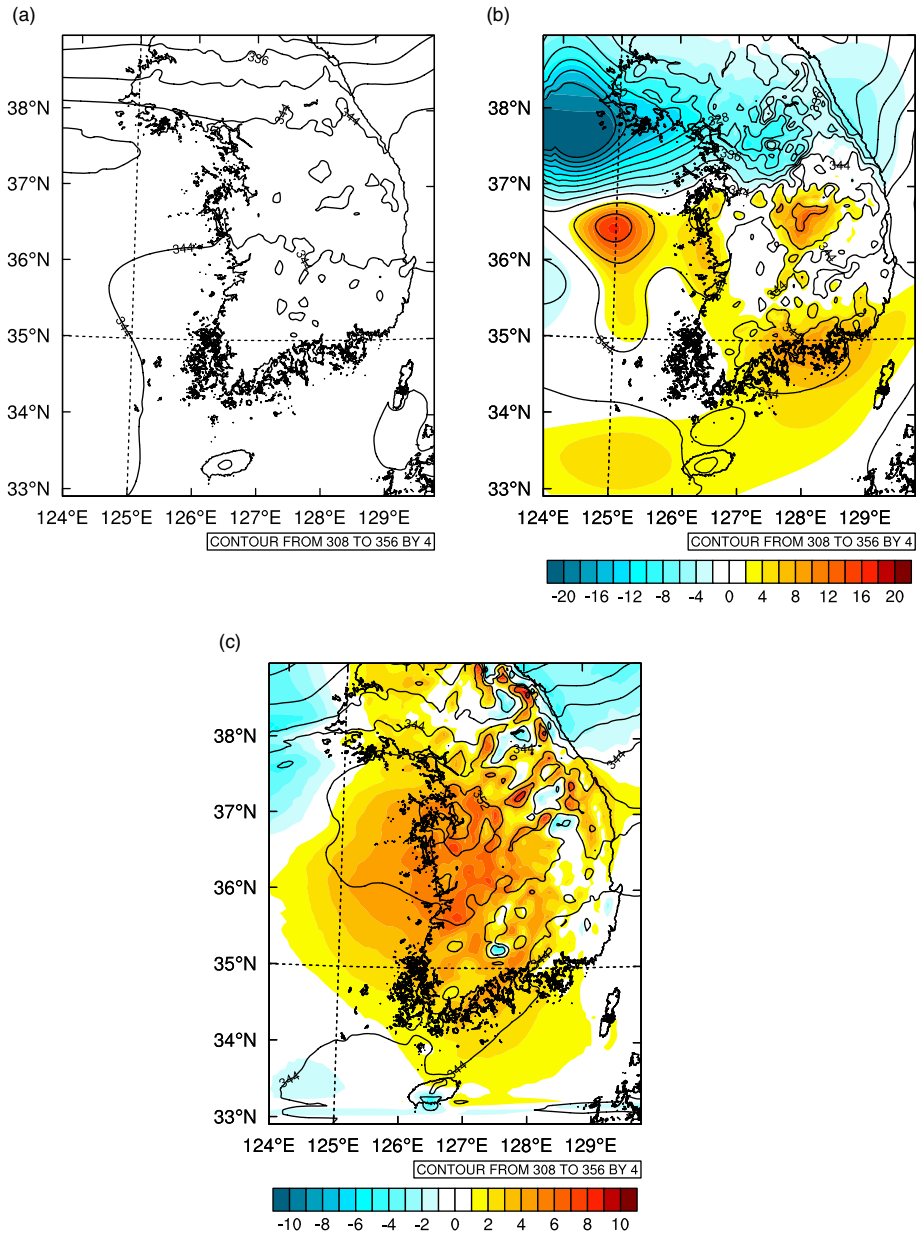

Fig. 11. Horizontal distributions of 850-hPa equivalent potential temperature (EPT) (contour interval of 4 K) at 1800 UTC 26 July 2006 for the (a) CONTROL, (b) 4DVAR, and (c) ASDA experiments. In case of data assimilation experiments, the analysis increments of EPT (shaded, K) are also shown.

forecast error is defined as the difference between the forecast from the original first guess and the verifying 3D-Var analysis at the end of the assimilation window, and an adjoint model is run backwards with the forecast-error gradient as input. The adjoint sensitivity of forecast error to the initial condition is scaled by an optimal scaling factor. The optimal scaling factor is determined by minimising the observational cost function of the 4D-Var method, and the scaled sensitivity is added to the original first guess. Finally, an improved analysis is made by carrying out 3D-Var with the improved first guess and the observations at the analysis time (or beginning of the assimilation window).

The simulated rainfall distribution is shifted northeastward compared to the observations when no radar data are assimilated or when radar data are assimilated using the 3D-Var method. The rainfall distribution and time series of rainfall are similar to the observations when radar data are assimilated using the 4D-Var method or ASDA method. Quantitative precipitation forecast (QPF) skill is also

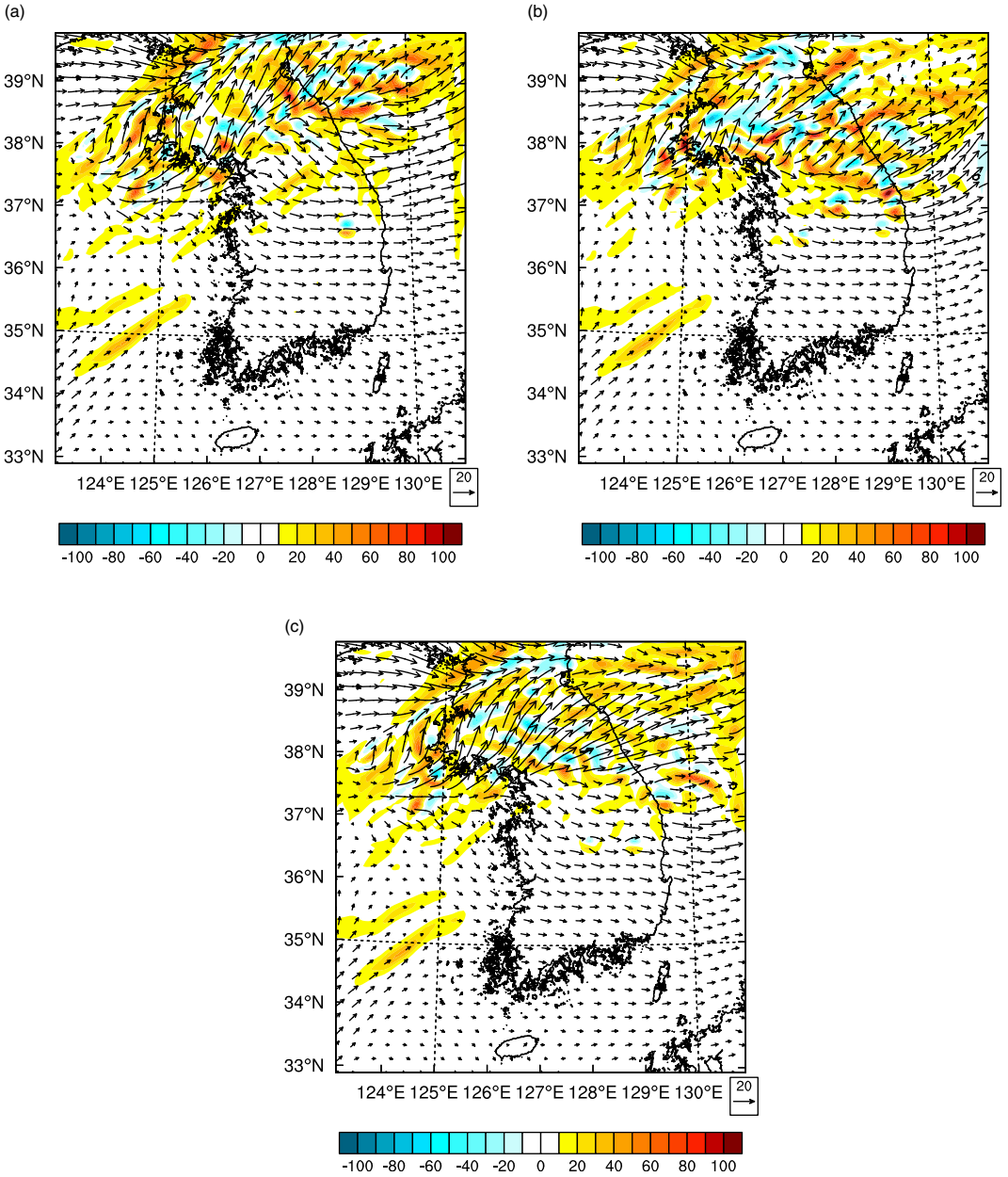

Fig. 12. Horizontal distributions of 500-hPa absolute vorticity (shaded, 10^{-5} s^{-1}) and vertical wind shear vector between 500 and 800 hPa (m s^{-1} hPa^{-1}) at 0600 UTC 27 July 2006 for the (a) CONTROL, (b) 4DVAR, and (c) ASDA experiments.

improved in the 4DVAR and ASDA experiments compared to the CONTROL and 3DVAR experiments according to analyses of TSs, BSs, and the RMSEs of rainfall. Simulated atmospheric fields such as zonal wind, meridional wind, temperature, and the water vapour mixing ratio are verified against the observational data. When the forecasts are verified against observational data like sounding data or radar radial velocity data, the fits to the observations or RMSEs of the 4DVAR and ASDA experiments are better than the CONTROL and 3DVAR experiments.

In conclusion, the heavy rainfall affecting the Korean Peninsula is not simulated well when radar data are assimilated using the 3D-Var method. The forecasts from 4D-Var analysis are similar to the observations, but the computational cost of the 4D-Var method is very high (due to iterative minimisation) compared to the 3D-Var method. Forecasts based on the proposed ASDA method are

also similar to the observations, and the characteristics of TL/AS- and BB-type MCSs are properly simulated. It should be noted that the computational cost of the ASDA method is relatively low (one non-linear-model/adjoint-model run, two 3D-Var analyses, scaling-factor determination), and that the first-guess and observations errors are not correlated with each other. The conclusions of this study cannot be generalised because the ASDA method was applied to only one particular case. The ASDA method will be applied to a variety of cases, including extreme weather conditions and daily fair weather conditions, and it will be compared to other data assimilation methods. We will also investigate the validity of the tangent linear approximation of moist physics using more cases. This will provide statistical evidence for the applicability of the ASDA method in an operational environment.

6. Acknowledgements

This work was funded by the Korea Meteorological Administration Research and Development Program under Grant CATER 2012-3062. This work was also supported by the Brain Korea 21 Plus Project (through the School of Earth and Environmental Sciences, Seoul National University). The third author, Dong-Kyou Lee was partially supported by Leading Foreign Research Institute Recruitment Program through the National Research Foundation of Korea funded by the Ministry of Science, ICT & Future Planning (MSIP) 2010-00715. The authors thank the anonymous reviewers for their valuable comments. Discussions with Dr. Xin Zhang at NCAR and Dr. Hyo-Jong Song at KIAPS were very helpful to this study.

References

Astling, E. G., Paegle, J., Miller, E. and O'Brien, C. J. 1985. Boundary layer control of nocturnal convection associated with a synoptic-scale system. *Mon. Wea. Rev.* **113**, 540–552.

Barker, D., Huang, X.-Y., Liu, Z., Auligne, T., Zhang, X. and co-authors. 2012. The Weather Research and Forecasting (WRF) model's community variational/ensemble data assimilation system: WRFDA. *Bull. Am. Meteorol. Soc.* **93**, 831–843.

Bjerknes, V. 1904. Das Problem der Wettervorhersage, betrachtet vom Standpunkt der Mechanik und der Physik. *Meteorol. Z.* **21**, 1–7.

Chen, T.-C. and Kpaeyeh, J. A. 1993. The synoptic-scale environment associated with the low-level jet of the great plains. *Mon. Wea. Rev.* **121**, 416–420.

Dudhia, J. 1989. Numerical study of convection observed during the winter monsoon experiment using a mesoscale two-dimensional model. *J. Atmos. Sci.* **46**, 3077–3107.

Gauthier, P., Tanguay, M., Laroche, S. and Pellerin, S. 2007. Extension of 3DVAR to 4DVAR: implementation of 4DVAR at the Meteorological Service of Canada. *Mon. Wea. Rev.* **135**, 2339–2364.

Gauthier, P. and Thépaut, J.-N. 2001. Impact of the digital filter as a weak constraint in the preoperational 4DVAR assimilation system of Météo France. *Mon. Wea. Rev.* **129**, 2089–2102.

Hello, G., Lalaurette, F. and Thépaut, J.-N. 2000. Combined use of sensitivity information and observations to improve meteorological forecasts: a feasibility study applied to the 'Christmas storm' case. *Q. J. Roy. Meteorol. Soc.* **126**, 621–647.

Honda, Y., Nishijima, M., Koizumi, K., Ohta, Y., Tamiya, K. and co-authors. 2005. A pre-operational variational data assimilation system for a non-hydrostatic model at the Japan Meteorological Agency: formulation and preliminary results. *Q. J. Roy. Meteorol. Soc.* **131**, 3465–3475.

Hong, S.-Y. and Lim, J.-O. 2006. The WRF single-moment 6-class microphysics scheme (WSM6). *J. Kor. Meteorol. Soc.* **42**, 129–151.

Hong, S.-Y., Noh, Y. and Dudhia, J. 2006. A new vertical diffusion package with an explicit treatment of entrainment processes. *Mon. Wea. Rev.* **134**, 2318–2341.

Huang, X.-Y. 1999. A generalization of using an adjoint model in intermittent data assimilation system. *Mon. Wea. Rev.* **127**, 766–787.

Huang, X.-Y., Gustafsson, N. and Källén, E. R. 1997. Using an adjoint model to improve an optimum interpolation-based data-assimilation system. *Tellus A.* **49**, 161–176.

Huang, X.-Y., Yang, X., Gustafsson, N., Mogensen, K. and Lindskog, M. 2002. *Four-Dimensional Variational Data Assimilation for a Limited Area Model*. Sweden, HIRLAM Tech Rep 57, Available from SMHI, S-601 76 Norrkoping, 41 pp.

Jiang, X., Lau, N.-C., Held, I. M. and Ploshay, J. J. 2007. Mechanisms of the great plain low-level jet as simulated in an AGCM. *J. Atmos. Sci.* **64**, 532–547.

Kain, J. S. 2004. The Kain-Fritsch convective parameterization: an update. *J. Appl. Meteorol.* **43**, 170–181.

Le Dimet, F. and Talagrand, O. 1986. Variational algorithms for analysis and assimilation of meteorological observations: theoretical aspects. *Tellus A.* **38**, 97–110.

Lewis, J. and Derber, J. 1985. The use of adjoint equations to solve a variational adjustment problem with advective constraints. *Tellus A.* **37**, 309–327.

McCorcle, M. D. 1988. Simulation of surface-moisture effects on the Great Plain low-level jet. *Mon. Wea. Rev.* **116**, 1705–1720.

Miller, L. J., Mohr, C. G. and Weinheimer, A. J. 1986. The simple rectification to Cartesian space of folded radial velocities from Doppler radar sampling. *J. Atmos. Ocean. Technol.* **3**, 162–174.

Mlawer, E. J., Taubman, S. J., Brown, P. D., Iacono, M. J. and Clough, S. A. 1997. Radiative transfer for inhomogeneous atmospheres: RRTM, a validated correlated-k model for the longwave. *J. Geophys. Res.* **102**, 16663–16682.

Mohr, C. G. and Vaughan, R. L. 1979. An economical procedure for Cartesian interpolation and display of reflectivity data in three dimensional space. *J. Appl. Meteorol.* **18**, 661–670.

Mohr, C. G., Vaughan, R. L. and Frank, H. W. 1986. The merger of mesoscale datasets into a common Cartesian format for efficient and systematic analyses. *J. Atmos. Ocean. Technol.* **3**, 144–161.

Park, S.-G. and Lee, D.-K. 2009. Retrieval of high-resolution wind fields over the Southern Korean Peninsula using the Doppler weather radar network. *Wea. Forecast.* **24**, 87–103.

Parrish, D. F. and Derber, J. 1992. The National Meteorological Center's spectral statistical-interpolation analysis system. *Mon. Wea. Rev.* **120**, 1747–1763.

Rabier, F., Järvinen, H., Klinker, E., Mahfouf, J.-F. and Simmons, A. 2000. The ECMWF operational implementation of four-dimensional variational assimilation. Experimental results with simplified physics. *Q. J. Roy. Meteorol. Soc.* **126**, 1143–1170.

Rabier, F., Klinker, E., Courtier, P. and Hollingsworth, A. 1996. Sensitivity of forecast errors to initial conditions. *Q. J. Roy. Meteorol. Soc.* **122**, 121–150.

Rawlins, F., Ballard, S. P., Bovis, K. J., Clayton, A. M., Li, D. and co-authors. 2007. The Met Office global 4-dimensional data assimilation system. *Q. J. Roy. Meteorol. Soc.* **133**, 347–362.

Skamarock, W. C., Klemp, J. B., Dudhia, J., Gill, D. O., Barker, D. M. and co-authors. 2008. *A Description of the Advanced Research WRF Version 3*. NCAR Tech. Note TN-475+STR, 113 pp.

Schumacher, R. S. and Johnson, R. H. 2005. Organization and environmental properties of extreme-rain-producing mesoscale convective systems. *Mon. Wea. Rev.* **133**, 961–976.

Schumacher, R. S. and Johnson, R. H. 2008. Mesoscale processes contributing to extreme rainfall in a midlatitude warm-season flash flood. *Mon. Wea. Rev.* **136**, 3964–3986.

Schumacher, R. S. and Johnson, R. H. 2009. Quasi-stationary, extreme-rain-producing convective systems associated with mid-level cyclonic circulation. *Wea. Forecast.* **24**, 555–574.

Talagrand, O. 1997. Assimilation of observations, an introduction. *J. Met. Soc. Jpn.* **75**, 191–209.

Tanguay, M., Fillion, L., Lapalme, E. and Lajoie, M. 2012. Four-dimensional variational data assimilation for the Canadian regional deterministic prediction system. *Mon. Wea. Rev.* **140**, 1517–1538.

Xiao, Q., Kuo, Y.-H., Sun, J., Lee, W.-C., Lim, E. and co-authors. 2005. Assimilation of Doppler radar observations with a regional 3DVAR system: impact of Doppler velocities on forecasts of a heavy rainfall case. *J. Appl. Meteorol.* **44**, 768–788.

Xu, L., Rosmond, T. and Daley, R. 2005. Development of NAVDAS-AR: formulation and initial tests for the linear problem. *Tellus A.* **57**, 546–559.

Zhang, X., Huang, X.-Y. and Pan, N. 2013. Development of the upgraded tangent linear and adjoint of the Weather Research and Forecasting (WRF) model. *J. Atmos. Ocean. Technol.* **30**, 1180–1188.